Monthly Notices
of the
ROYAL ASTRONOMICAL SOCIETY

MNRAS **508,** 3463–3473 (2021)
Advance Access publication 2021 October 1

https://doi.org/10.1093/mnras/stab2818

Exploring black hole scaling relations via the ensemble variability of active galactic nuclei

A. Georgakakis [1]★ I. Papadakis[2,3] and M. Paolillo [4,5,6]

[1] *Institute for Astronomy & Astrophysics, National Observatory of Athens, V. Paulou & I. Metaxa 11532, Greece*
[2] *Department of Physics and Institute of Theoretical and Computational Physics, University of Crete, 71003 Heraklion, Greece*
[3] *Institute of Astrophysics, Foundation for Research and Technology, 71110 Heraklion, Greece*
[4] *Dipartimento di Fisica 'Ettore Pancini', Università Federico II, via Cinthia, I-80126 Napoli, Italy*
[5] *INAF - Osservatorio Astronomico di Capodimonte, via Moiariello 16, I-80131 Napoli, Italy*
[6] *Istituto Nazionale di Fisica Nucleare, Sezione di Napoli, I-80126 Napoli, Italy*

Accepted 2021 September 27. Received 2021 August 8; in original form 2021 May 18

ABSTRACT

An empirical model is presented that links, for the first time, the demographics of active galactic nuclei (AGN) to their ensemble X-ray variability properties. Observations on the incidence of AGN in galaxies are combined with (i) models of the power spectrum density (PSD) of the flux variations of AGN and (ii) parametrizations of the black hole mass versus stellar mass scaling relation to predict the mean excess variance of active black hole populations in cosmological volumes. We show that the comparison of the model with observational measurements of the ensemble excess variance as a function of X-ray luminosity provides a handle on both the PSD models and the black hole mass versus stellar mass relation. We find strong evidence against a PSD model that is described by a broken power law and a constant overall normalization. Instead, our analysis indicates that the amplitude of the PSD depends on the physical properties of the accretion events, such as the Eddington ratio and/or the black hole mass. We also find that current observational measurements of the ensemble excess variance are consistent with the black hole mass versus stellar mass relation of local spheroids based on dynamically determined black hole masses. We also discuss future prospects of the proposed approach to jointly constrain the PSD of AGN and the black hole mass versus stellar mass relation as a function of redshift.

Key words: galaxies: active – galaxies: nuclei – quasars: supermassive black holes – X-rays: general.

1 INTRODUCTION

One of the fundamental properties of the accretion flows on to supermassive black holes (SMBHs) are the stochastic variations of the radiated flux. These occur on a wide range of time scales and provide information on the size of the central source (e.g. Lynden-Bell 1969) and the physics of the accretion process (e.g. Rees 1984). The origin of these variations is still under discussion and could be related to instabilities of the accretion flow, a flaring corona or hotspots orbiting the central compact object (e.g. Gravity Collaboration 2018, 2020). Whatever the nature of the underlying physical mechanism, observations, particularly at X-rays, point to a common process for the flux variability of active black holes over a broad range of masses and accretion rates (e.g. McHardy et al. 2006; Körding et al. 2007a). This is manifested by remarkable similarities in the statistical measures of the observed flux variations [e.g. power spectrum density (PSD)] of different objects, once the key physical parameters of individual systems, such as the mass of the compact object and/or the Eddington ratio of the accretion flow, are factored out (e.g. González-Martín & Vaughan 2012; Ponti et al. 2012). These similarities extend from supermassive black holes in active galactic nuclei (AGN) to stellar size black holes in binary systems (e.g. McHardy et al. 2006), thereby indicating common variability mechanisms over many orders of magnitude in mass. The implication of this observational fact is that the amplitude of the variability on different time scales provides a handle on the physical properties of the accreting system. For example, flux variations, particularly at X-rays, have being proposed as a means of measuring the black hole masses of AGN (e.g. Czerny et al. 2001; Nikolajuk, Papadakis & Czerny 2004; Ponti et al. 2012) in a way that is complementary to dynamical estimates.

In addition to studies of the light curves of individual objects, it has also been shown that there is value in measuring the mean variability properties of AGN populations detected in extragalactic X-ray survey fields (Paolillo et al. 2004; Papadakis et al. 2008; Paolillo et al. 2017). These measurements are taking advantage of the fact that in many popular survey fields the total integration time has been gradually built up by numerous repeat observations carried out over the course of many years (e.g. 7 Msc *Chandra* Deep Field South, Luo et al. 2017). Although the light curves of individual sources in such surveys carry limited information, the ensemble of all AGN provides useful constraints on the integrated variability power of the population (Allevato et al. 2013). Such observations have enabled investigations on the redshift evolution of the AGN variability properties (e.g. Papadakis et al. 2008) and the dependence of the flux variability amplitude on observables such as the accretion luminosity (e.g. Paolillo et al. 2017). Moreover, because of the dependence of the

★ E-mail: age@noa.gr

variability power spectrum on the physical properties of the active black holes, measurements of the ensemble flux variations of AGN contain information on the distribution of Eddington ratios and black hole masses of the population (e.g. Allevato et al. 2010; Paolillo et al. 2017).

The latter two quantities are also relevant to investigations of the accretion history of the Universe and the co-evolution of AGN and their host galaxies. Observational studies on the incidence of AGN in galaxies, for example, associate proxies of the Eddington ratio distribution to the properties of AGN hosts (e.g. star formation rate, stellar mass) to explore the physical conditions that promote accretion events on to SMBHs (e.g. Kauffmann & Heckman 2009; Azadi et al. 2015; Georgakakis et al. 2017; Aird, Coil & Georgakakis 2018, 2019). Also, the continuity equation of the black hole mass function uses the observed AGN luminosity function as boundary condition to determine the growth history of SMBHs, infer the Eddington ratio distribution of AGN and constrain black hole fuelling models (e.g. Merloni & Heinz 2008; Shankar, Weinberg & Miralda-Escudé 2013; Aversa et al. 2015). Observational measurements of the ensemble variability of AGN could feedback to the studies above by providing an independent observational handle on the Eddington ratio and black hole mass distributions of the population.

In this paper, we build upon this potential to link the mean variability of AGN populations to black hole demographics. A new empirical model is developed that combines observational results on the occupation of galaxies by AGN with models of their variability amplitude on different time scales. This is used to make predictions on the mean variability of AGN populations as a function of observables, such as accretion luminosity and redshift. A forward modelling approach is then used to compare the predictions with observations. We demonstrate the predictive power of the model and show how it can jointly constrain models of the AGN variability amplitude and the black hole mass versus stellar mass relation of the population.

Sartori et al. (2018, 2019) also proposed a forward modelling methodology for interpreting AGN variability observations and constraining variability models. One of the differences of our approach compared to these previous studies is that our work directly includes information based on AGN demographics.

2 MODEL CONSTRUCTION

The focus of this work is the modelling of the stochastic (intrinsic) variations of the luminosity of AGN that occur on different time scales. There are two quantities that are relevant for this exercise, the PSD and the normalized excess variance $\sigma^2_{\rm NXV}$ (Nandra et al. 1997). The PSD describes the distribution of the variance of a light curve in Fourier frequencies. The $\sigma^2_{\rm NXV}$ is a commonly used statistic for measuring the variability of light curves. This quantity relates to the PSD via an integration in frequencies (see Section 2.4). It is also the end product of our modelling. It is assumed that the PSD can be approximated with a broken power law functional form with parameters (i.e slopes, break frequency, normalization) that depend on the physical properties of the system (see Section 2.4), such as the mass of the black hole and the accretion rate on to it (e.g. McHardy et al. 2006; Körding et al. 2007b; Ponti et al. 2012).

Fig. 1 graphically demonstrates the construction of the AGN ensemble-variability model that relies solely on empirical relations. The starting point is a mock galaxy sample drawn from a stellar mass function (panel 1 of Fig. 1; see Section 2.1 for details). The mock galaxies are seeded with AGN using observationally determined AGN specific accretion rate distributions, $P(\lambda)$ (panel 2 of Fig. 1 and Section 2.2; e.g. Georgakakis et al. 2017; Aird et al. 2018), which measure the probability of a galaxy hosting an accretion event with specific accretion rate $\lambda \propto L_X/M_\star$. In this definition L_X is the X-ray luminosity of the event (AGN) in a given spectral band and $M_\star$ is the stellar mass of the host galaxy. The specific accretion rate is a purely observationally derived parameter and measures how much X-rays an AGN emits relative to the stellar mass of its host galaxy. The feature of the specific accretion rate distribution, $P(\lambda)$, is that it is a measure of the incidence of AGN among galaxies. Therefore, it can be applied in a probabilistic way to a galaxy sample (see panel 1/Fig. 1) and seed them with AGN (see panel 3/Fig. 1). Mathematically, this seeding process is described by the convolution of the stellar mass function of galaxies (a well-constrained observable, e.g. Weigel, Schawinski & Bruderer 2016) with the specific accretion rate distribution. The process described above produces a mock sample of AGN, each of which is assigned an X-ray luminosity, host galaxy stellar mass, and redshift (L_X, $M_\star$, z).

Next a parametrization of the black hole mass versus stellar mass relation is introduced (panel 4 of Fig. 1; see Section 2.3). Each mock AGN with stellar mass, $M_\star$, is assigned a black hole mass, $M_{\rm BH}$, and given the X-ray luminosity, L_X, an Eddington ratio $\lambda_{\rm EDD} \propto L_X/L_{\rm EDD}$, where $L_{\rm EDD}$ is the Eddington luminosity. We then use observationally motivated analytic models that describe the PSD and its dependence on black hole mass and/or Eddington ratio (see panel 5 of Fig. 1; Section 2.4) to assign each mock AGN a variability power spectrum. It is then straightforward to determine for each AGN an excess variance by integrating the corresponding PSD.

We are interested in the ensemble (mean) excess variance of the AGN population rather than the variability properties of individual systems. The panel 6 of Fig. 1 shows the parameter space that will be used in later sections to compare the model predictions against the observations. It plots the ensemble variance of AGN as a function of X-ray luminosity. The data points on this plot are measurements of the mean $\sigma^2_{\rm NXV}$ of AGN in the *Chandra* Deep Field South field (Paolillo et al. 2017). On the model side, the population of mock AGN is binned by X-ray luminosity to yield the mean (ensemble) excess variance as a function of L_X. In the next sections, we describe in detail each of the components of the ensemble variability model that is graphically demonstrated in Fig. 1.

2.1 The stellar mass function

For the stellar mass function of galaxies, we adopt the double Schechter function parametrization presented by Ilbert et al. (2013) based on observations in the COSMOS survey field (Scoville et al. 2007). They provide analytic fits to the galaxy mass function in discrete redshift intervals between $z = 0.2$ and $=4$. These are interpolated/extrapolated to yield a continuous sampling of the mass function in the redshift range $z = 0-4$. Below the redshift limit of $z = 0.2$, the mass function is fixed to the parametrization of the lower redshift bin of Ilbert et al. (2013). The resampled mass functions define a 2D surface in the stellar mass versus redshift space. This is used to randomly draw pairs of $M_\star$ and z that are distributed in the above 2D space according to the observations. This sequence of pairs represents the mock galaxy sample.

2.2 Specific accretion rate distribution

Mock galaxies are seeded with specific accretion rates λ, using the probability density distributions, $P(\lambda)$, presented by Georgakakis, Ruiz & LaMassa (2020). The latter are approximated by a broken

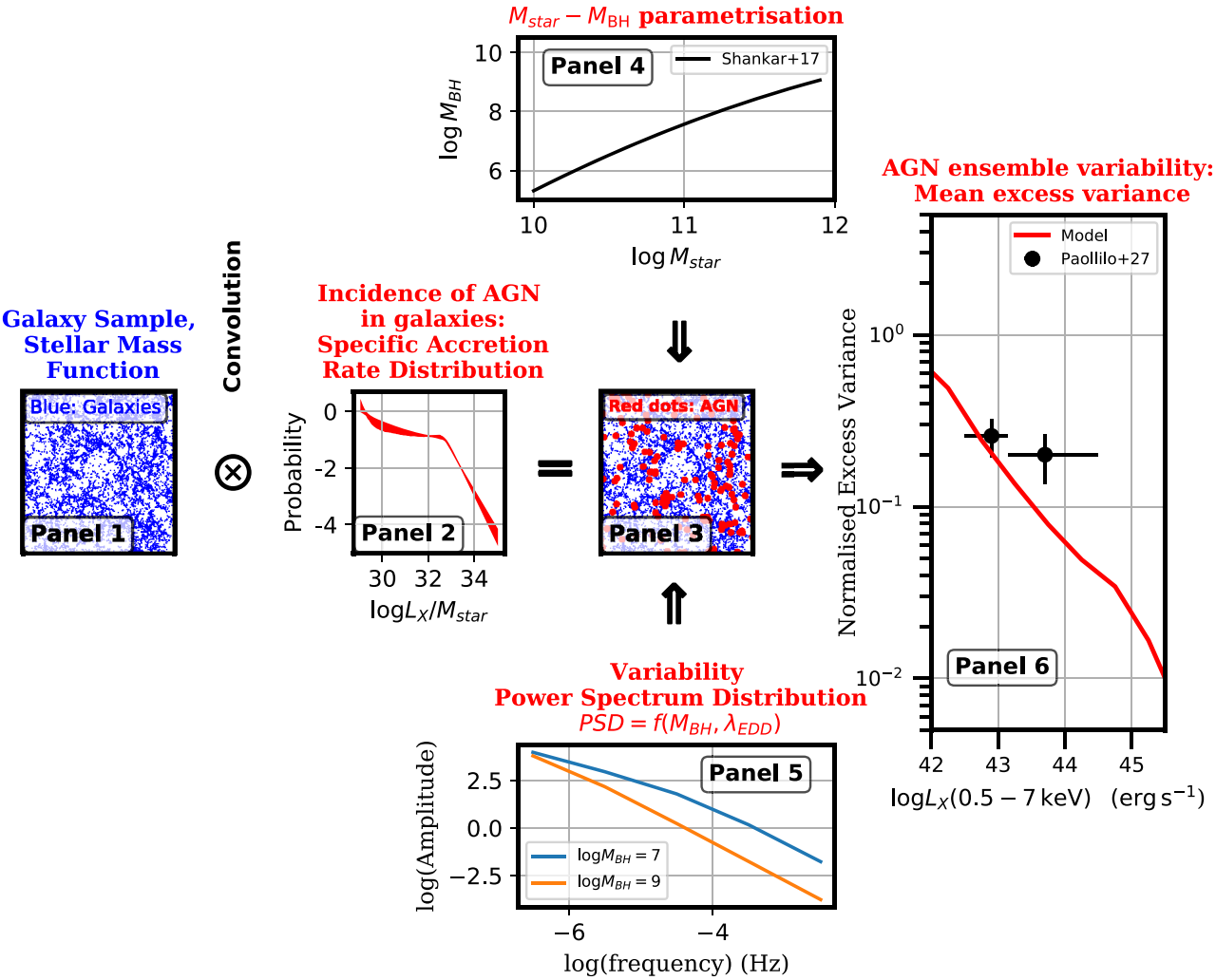

Figure 1. Flowchart of the empirical AGN variability model. The blue dots in panel 1 represent galaxies distributed in a cosmological volume that are drawn from the stellar mass function (Ilbert et al. 2013). They are seeded with AGN specific accretion rates ($\lambda \propto L/M_\star$) using the corresponding observationally derived probability distribution functions, e.g. those shown in panel 2. This produces a sample of mock AGN (the red dots of panel 3), each of which has been assigned an X-ray luminosity, L_X, a host-galaxy stellar mass, $M_\star$, and a redshift, z. A parametrization of the $M_\star - M_{BH}$ correlation (panel 4) is used to assign black holes to mock AGN and hence, Eddington ratios $\lambda_{\rm EDD} \propto L_X/M_{\rm BH}$. The dependence of the AGN variability power spectrum density (PSD; panel 5) on black hole mass and Eddington ratio is then used to assign variability to each mock AGN. It is then straightforward to determine for each AGN an excess variance ($\sigma^2_{\rm NXV}$) by integrating the corresponding PSD. The average excess variance of the population binned in luminosity and redshift intervals (the solid line in panel 6) can then be directly compared with observational results (the black points in panel 6; Paolillo et al. 2017).

power law with parameters determined by requiring that the convolution of the $P(\lambda)$ with the galaxy stellar mass function of Ilbert et al. (2013) yields the total X-ray luminosity function measured by Aird et al. (2015). Each mock galaxy with stellar mass $M_\star$ is assigned a specific accretion rate, $\lambda \propto L_X/M_\star$, which is drawn from the distributions presented by Georgakakis et al. (2020). The intrinsic (i.e. corrected for obscuration) X-ray luminosity of a given mock AGN is estimated as $L_X = \lambda \times M_\star$, where in this application the L_X corresponds to the 2–10 keV spectral band.

In the following sections, the X-ray fluxes of mock AGN will also be required. This is to mimic the observational selection effects of flux-limited AGN samples and provide a meaningful comparison between the model predictions with the observations. The determination of model fluxes requires knowledge of the level obscuration of individual mock AGN that absorbs their intrinsic luminosities. An X-ray spectral model is also needed to convert luminosities to fluxes.

Obscured AGN are accounted for in the estimation of the X-ray luminosity function of Aird et al. (2015) and are therefore included in our modelling. The AGN obscuration is parametrized by the atomic hydrogen column density, $N_{\rm H}$. The distribution of AGN in $N_{\rm H}$ is a function of both accretion luminosity and redshift following the model presented by Aird et al. (2015). Compton thick AGN with $N_{\rm H} > 10^{24}$ cm^{-2} are also included in this model. Their space density is assumed to be 34 per cent of moderately obscured active black holes, i.e. those with $N_{\rm H} = 10^{22}$–10^{24} cm^{-2}. The Aird et al. (2015) model distribution is sampled in a probabilistic way using a Monte Carlo approach to assign mock AGN line-of-sight atomic hydrogen column densities.

Using the $N_{\rm H}$, z, $L_{\rm X}$(2–10 keV) assigned to mock AGN it is then also possible to estimate the corresponding flux in any observed energy band. This calculation follows the methodology described in Georgakakis et al. (2020). The adopted X-ray spectrum consists of an intrinsic power law that is transmitted through an obscuring

medium that absorbs and scatters the X-ray photons. We use the torus model of Brightman & Nandra (2011) to describe these processes and produce the resulting X-ray spectra. This model assumes a sphere of constant density with two symmetric conical wedges with vertices at the centre of the sphere removed. The opening angle of the cones is fixed to 45° and the viewing angle of the observer is set to 87°, i.e. nearly edge on. The spectral index of the intrinsic power-law is assumed to be $\Gamma = 1.9$ (e.g. Nandra et al. 1997).

2.3 Relation between stellar and black hole mass

Two different parametrizations of the black hole versus stellar mass relation are adopted. The first is based on dynamically measured black hole masses at the centres of local non-active galaxies, i.e. those with dormant black holes. We use the scaling relation

$$\log \frac{M_{\rm BH}}{\rm M_\odot} = 8.35 + 1.31 \left(\log \frac{M_\star}{\rm M_\odot} - 11 \right), \quad (1)$$

which is derived by Shankar et al. (2020) based on the sample of early and late-type galaxies with dynamical black hole mass estimates presented by Savorgnan et al. (2016). The coefficients of the relation above are estimated using all the galaxies in the sample of Savorgnan et al. (2016). The intrinsic rms scatter in the $\log M_{\rm BH}$ direction is 0.5 dex.

Evidence has been emerging recently suggesting that the scaling relations based on dynamical black hole mass estimates, like the one in equation (1), may be biased (Bernardi et al. 2007; Shankar et al. 2016). This is because the gravitational sphere of influence of supermassive black holes has to be resolved to estimate their masses via dynamical arguments. At the spatial resolution limit of current instrumentation, this is feasible only for the subset of local galaxies that host the most massive black holes at fixed stellar mass (Shankar et al. 2016). It is argued that this selection effect distorts the inferred normalization and/or shape of the local scaling relations between stellar mass proxies and black hole masses (Shankar, Bernardi & Sheth 2017). We explore the impact of this potential source of bias on the modelling of the AGN variability by also considering the intrinsic (unbiased) scaling relation proposed by Shankar et al. (2016):

$$\begin{aligned} \log \frac{M_{\rm BH}}{\rm M_\odot} &= 7.574 + 1.946 \left(\log \frac{M_\star}{\rm M_\odot} - 11 \right) \\ &\quad - 0.306 \left(\log \frac{M_\star}{\rm M_\odot} - 11 \right)^2 \\ &\quad - 0.011 \left(\log \frac{M_\star}{\rm M_\odot} - 11 \right)^3 . \end{aligned} \quad (2)$$

In the relation above the black hole mass logarithmic scatter is assumed to depend on $M_\star$ as in Shankar et al. (2016):

$$\sigma_{\rm BH} = 0.32 - 0.1 \left(\log \frac{M_\star}{\rm M_\odot} - 12 \right). \quad (3)$$

It is cautioned that the stellar mass in the relations above should represent that of the bulge, $M_{\rm bulge}$, not the total of the galaxy. Equations (1) and (2) therefore assume that $M_\star \approx M_{\rm bulge}$. This approximation breaks down in the case of late-type and/or bulgeless galaxies. As an example, spiral galaxies of the Sb/Sbc type have typical bulge to total stellar mass ratios $M_{\rm bulge}/M_\star \approx 0.5$ (e.g Fukugita, Hogan & Peebles 1998; Oohama et al. 2009). The impact of this effect on the results will be investigated in later sections.

Equations (1) and (2) will be used independently to seed galaxies with black holes and produce distinct predictions on the variability amplitude of the resulting samples. For a given black hole mass the corresponding Eddington ratio is $\lambda_{\rm Edd} = L_{\rm bol}/L_{\rm Edd}$, where $L_{\rm Edd}$ is the Eddington luminosity. The bolometric luminosity, $L_{\rm bol}$, is estimated from the 2–10 keV X-ray luminosity using the bolometric correction of Duras et al. (2020) for their combined Type-1 and Type-2 AGN sample.

2.4 Variability model parametrization

X-ray monitoring campaigns of a few dozen luminous AGN show that their PSDs can be approximated with a double power-law functional form with a slope of about –2 at high frequencies that flattens to –1 at the low-frequency end (e.g. Papadakis et al. 2002; Uttley, McHardy & Papadakis 2002; Markowitz et al. 2003; McHardy et al. 2007). We therefore parametrize the PSD with a bending power law of the form

$$PSD(\nu) = A\, \nu^{-1} \left(1 + \frac{\nu}{\nu_b} \right)^{-1}, \quad (4)$$

similar to that proposed by McHardy et al. (2004, see also González-Martín & Vaughan 2012) based on local AGN observations. In the equation above, A is the normalization factor and $\nu_{\rm b}$ is the bending frequency, where the power-law slope changes from -1 at the limit $\nu << \nu_{\rm b}$ to -2 for $\nu >> \nu_{\rm b}$. The equation above can be integrated to yield the flux variance:

$$\begin{aligned} \sigma^2_{\rm mod} &= \int_{\nu_{\rm min}}^{\nu_{\rm max}} PSD(\nu)\, {\rm d}\nu \\ &= A \left(\ln \frac{\nu_{\rm max}}{\nu_{\rm min}} - \ln \frac{\nu_{\rm b} + \nu_{\rm max}}{\nu_{\rm b} + \nu_{\rm min}} \right), \end{aligned} \quad (5)$$

where the integration limits $\nu_{\rm min}$, $\nu_{\rm max}$ are the lowest and highest rest-frame frequencies sampled by the observed light curve. These are estimated from the relations

$$\nu_{\rm min} = \frac{1+z}{\Delta t^{obs}_{\rm max}}, \quad (6)$$

$$\nu_{\rm max} = \frac{1+z}{\Delta t^{obs}_{\rm min}}, \quad (7)$$

where z is the redshift and $\Delta t^{obs}_{\rm min}$, $\Delta t^{obs}_{\rm max}$ are, respectively, the minimum sampled time scale and the total duration of the light curve at the observer's frame.

The parameters of the PSD function of equation (4; i.e A, $\nu_{\rm b}$) are linked to the physical properties of AGN, such as the black hole mass and the Eddington ratio, using the four observationally motivated models discussed by Paolillo et al. (2017).

In the first model (Model 1) the PSD amplitude is constant for all AGN

$$A = 2 \cdot \nu_{\rm b} \cdot PSD(\nu_{\rm b}) = 0.02. \quad (8)$$

and the break frequency scales with the mass of the black hole as

$$\nu_{\rm b} = \frac{580}{M_{\rm BH}/{\rm M_\odot}} \left({\rm s}^{-1} \right). \quad (9)$$

These assumptions are based on the observational results of Papadakis (2004) and González-Martín & Vaughan (2012).

The second model (Model 2) also assumes a constant PSD amplitude as in Model 1, but the break frequency depends on both the black hole mass and the accretion rate as proposed by McHardy et al. (2006). This dependence is expressed in terms of the AGN bolometric luminosity:

$$\nu_{\rm b} = \frac{200}{86400} \cdot \frac{L_{\rm bol}}{10^{44}} \cdot \left(\frac{M_{\rm BH}}{10^6\, {\rm M_\odot}} \right)^{-2} \left({\rm s}^{-1} \right), \quad (10)$$

where $L_{\rm bol}$ is the bolometric luminosity in units of erg s^{-1} and the black hole mass is measured in solar units.

The third Model (Model 3) is a variation of Model 1 in that the assumption of a constant PSD amplitude is relaxed. Following the observational results of Ponti et al. (2012), the amplitude is assumed to scale with the Eddington ratio, $\lambda_{\rm Edd}$, of the accretion flow as

$$A = 2 \cdot \nu_{\rm b} \cdot PSD(\nu_{\rm b}) = 3 \times 10^{-2} \cdot \lambda_{\rm Edd}^{-0.8}. \quad (11)$$

The break frequency of Model 3 depends on black hole mass as in equation (9).

Finally, the fourth model (Model 4) is a mix of Models 2 and 3. The break frequency scales with black hole mass as in equation (10) and the PSD normalization depends on Eddington ratio via equation (11).

Allevato et al. (2013) showed that the normalized excess variance measured from AGN light curves with uneven and/or sparse sampling is not a direct measure of $\sigma^2_{\rm mod}$ as defined in equation (5) in the case of PSDs given by equation (4). Instead, the normalized excess variance is an estimator of the quantity $\sigma^2_{\rm obs}$ defined as

$$\sigma^2_{\rm obs} = \frac{\sigma^2_{\rm mod}}{C \cdot 0.48^{\beta-1}}. \quad (12)$$

The parameter β depends on the PSD slope below $\nu_{\rm min}$ and C is a correction factor that depends on the sampling pattern. Equation (5) is used to determine the $\sigma^2_{\rm mod}$ of mock AGN. This is then plugged into equation (12) to estimate $\sigma^2_{\rm obs}$, which is used to compare against the observational results.

3 MODELLING THE OBSERVATIONS

3.1 The *Chandra* Deep Field South data set

In this paper, we use the observational measurements of the AGN ensemble excess variance in the 7 Ms *Chandra* Deep Field South (CDFS, Luo et al. 2017) presented by Paolillo et al. (2017). This data set consists of 102 individual *Chandra* pointings split into multiple epochs over a period of 17 yr. It currently represents the state of the art in temporal studies of AGN populations because of the large number of repeat observations and their long time span.

We compare the model predictions with the excess variance measurements of the full sample of Paolillo et al. (2017) grouped into a single broad redshift bin, $z = 0.4{-}4.0$. They also presented variability measurements in narrower redshift intervals, $z = 0.4{-}1.03$, $1.03{-}1.8$, $1.8{-}2.75$, and $2.75{-}4$. We choose not to use these subsamples because of the larger uncertainties of individual data points and the narrower luminosity baseline. Additionally, the adopted modelling methodology allows to properly account for the sources' redshift distribution without the need to introduce binning. The excess variance of individual sources is measured from the light curves that span a time scale of 6205 d and include all the epochs of the 7 Ms CDFS observations.

The CDFS variability measurements of Paolillo et al. (2017) are limited to CDFS sources with signal-to-noise ratio >0.8. This is nearly equivalent to selecting sources with >350 net counts in the 0.5−7 keV spectral band of the coadded CDFS observations. For fainter sources, the Poisson noise dominates over the intrinsic variability. The thresholds above refer to the photon counts extracted within an aperture of variable size across the CDFS field of view that roughly corresponds to the 95 per cent encircled energy fraction (EEF; Giacconi et al. 2002; Paolillo et al. 2017). In the analysis that follows the 0.5–7 keV threshold of 350 net counts is adopted as the sample selection function. This limit cuts through the black hole mass and Eddington ratio parameter space and therefore affects the expected excess variance of the detected sources as well as that of the ensemble. It is therefore necessary to apply the count limit above to the mock AGN sample to mimic the CDFS 7 Ms observational selection effects. The adopted method for achieving this is discussed below.

3.2 Modelling the CDFS selection function

The conversion of the 0.5–7 keV flux of mock AGN to the observed photon counts on the *Chandra* ACIS-I detector assumes a power-law spectral model with index $\Gamma = 1.4$ that is absorbed by the Galactic hydrogen column density in the direction of the CDFS, $N_{\rm H} = 8.8 \times 10^{19}$ cm^{-2} (Luo et al. 2017). The choice of $\Gamma = 1.4$ is because Luo et al. (2017) adopt this value to construct the exposure maps of the CDFS, which are used in this calculation. The net counts of a source with a given flux depend on its position within the CDFS field of view. The maximum exposure is achieved close to the centre of the field and then drops smoothly towards the edges as a result of vignetting. Therefore, at fixed flux more counts are expected close to the CDFS centre compared to the field edges. It is possible to estimate the CDFS area over which a source with a given flux has more than 350 net counts within an aperture that includes 95 per cent of the source photons. The fraction of this area relative to the total of the CDFS field provides a measure of the probability that sources with the flux in question are included in the Paolillo et al. (2017) variability sample, i.e. the observational selection function. Using the CDFS 0.5–7 keV exposure map[1] and the spectral model above the expected net counts within the 95 per cent EEF aperture is

$$C = f_X(0.5{-}7\,{\rm keV}) \cdot t \cdot ECF \cdot 0.95, \quad (13)$$

where t represents the distribution of the exposure-map pixel values, $f_X(0.5{-}7\,{\rm keV})$ is the energy flux in the 0.5–7 keV band, and the ECF is the energy to photon flux conversion factor. For the adopted spectral model $ECF = 3.23 \times 10^{-9}$. The fraction of the exposure map pixels that yield $C > 350$ measure the CDFS fractional area within which a source with $f_X(0.5{-}7\,{\rm keV})$ has sufficient counts to be included in the variability sample of Paolillo et al. (2017). This fraction is plotted as a function of $f_X(0.5{-}7\,{\rm keV})$ in Fig. 2. This curve is used to assign weights to each source in the mock catalogue and generate samples that match the Paolillo et al. (2017) selection.

Next, we assess the ability of the selection function of Fig. 2 to reproduce the basic observational properties of the variability sample of CDFS AGN used in our analysis. Fig. 3 plots the distribution on the $L_X{-}z$ plane of mock AGN in the redshift interval $z = 0.4{-}4.0$ after filtering with the selection function curve of Fig. 2. The 7 Ms CDFS AGN (Luo et al. 2017) in the same redshift range and with full-band net counts >350 are also plotted in Fig. 3 for comparison. Overall, there is fair overlap in the distribution of mock and real AGN on the $L_X{-}z$ parameter space. This suggests that the selection function curve of Fig. 2 provides a reasonable representation of the observational selection effects of the 7 Ms CDFS field. This is further explored in Figs 4 and 5 that compare the redshift and luminosity distributions of mock AGN with the CDFS observations. The observed redshift peaks in Fig. 4 trace the substruture of the cosmic web along the CDFS line of sight, which is absent from the model. The observations also find a lower fraction of AGN in the interval $z = 0.5{-}1.5$ compared to the model prediction. Poisson uncertainties and cosmic variance are

[1] https://personal.psu.edu/wnb3/cdfs/cdfs-chandra.html

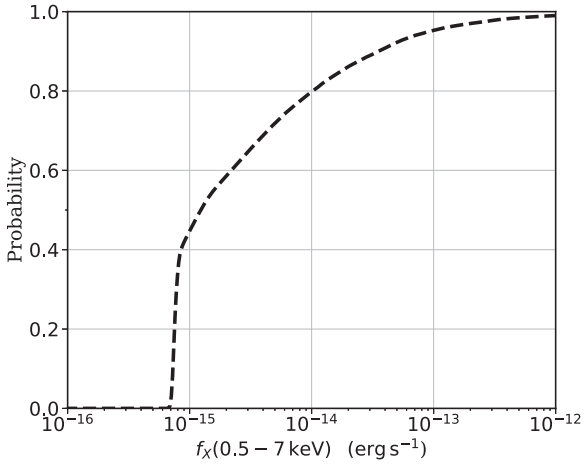

Figure 2. The selection function applied to the mock AGN sample. The vertical axis is the probability of an X-ray source with a given 0.5–7 keV flux to have more than 350 net counts within the CDFS field of view. This probability is plotted as a function of the 0.5–7 keV flux on the horizontal axis. The curve is designed to mimic the selection of the Paolillo et al. (2017) CDFS variability sample.

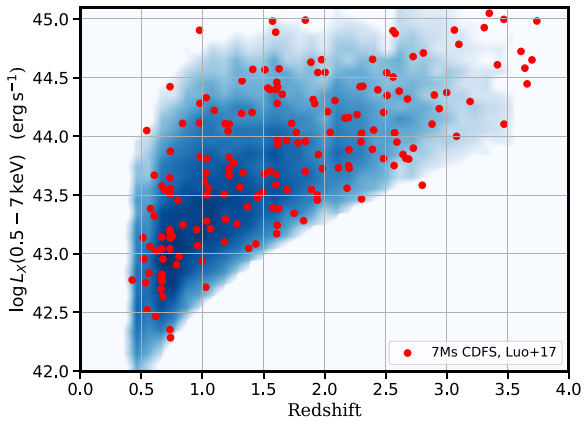

Figure 3. X-ray luminosity versus redshift parameter space. The red data points are the X-ray sources in the 7 Ms CDFS catalogue of Luo et al. (2017) in the redshift interval $z = 0.4-4$ and with full-band net counts >350. These criteria mimic the selection function of the Paolillo et al. (2017) variability sample. The blue-shaded region corresponds to mock AGN in the redshift interval above and filtered through the selection function curve plotted in Fig. 2. Darker shades of blue correspond to a higher density of mock AGN.

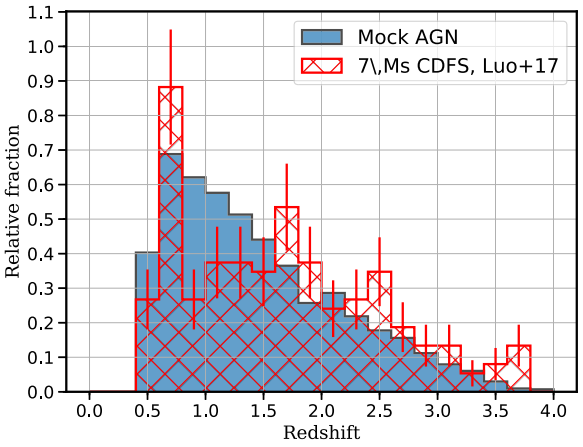

Figure 4. The redshift distribution of the 7 Ms CDFS sources (red-hatched histogram) shown in Fig. 3. The error bars of individual bins correspond to the Poisson uncertainty. The blue histogram is the projection of the 2D mock AGN distribution of Fig. 3 on to the redshift axis. Both the blue- and red-hatched histograms are normalized to unity.

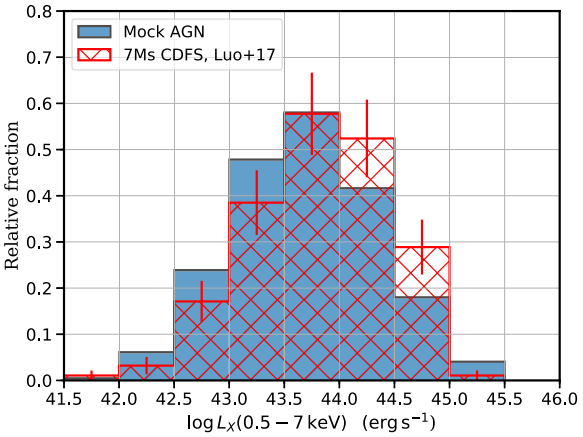

Figure 5. The X-ray luminosity distribution of the 7 Ms CDFS sources (red-hatched histogram) shown in Fig. 3. The error bars of individual bins correspond to the Poisson uncertainty. The blue histogram is the projection of the 2D mock AGN distribution of Fig. 3 on to the X-ray luminosity axis. Both the blue- and red-hatched histograms are normalized to unity.

likely responsible for this difference. Nevertheless, the model tracks reasonably well the high-redshift tail of the observations. In Fig. 5, there is evidence for an excess of luminous AGN in the observations compared to the model predictions. This is largely because of the differences in the redshift distribution of the model and observations in Fig. 4. The evidence above shows that the selection function curve of Fig. 2 reproduces at least to the first approximation the observational biases of the 7 Ms CDFS sample used by Paolillo et al. (2017).

3.3 Constructing the CDFS variability model

The galaxy stellar mass function of Section 2.1 is used to generate a sample of galaxies in the redshift interval $z = 0.4-4$ that corresponds to the Paolillo et al. (2017) CDFS variability sample. These are assigned specific accretion rates, X-ray luminosities, and hydrogen column densities as explained in Section 2.2. X-ray fluxes in the 0.5–7 keV band are also estimated at this stage. The mock AGN are seeded with black holes using the scaling relations of Section 2.3. Eddington ratios are also estimated for individual systems. For each mock AGN, the four PSD models of Section 2.4 are integrated between the lowest and highest rest-frame frequencies sampled by the 7 Ms CDFS light curves as defined by equations (6) and (7; $\Delta t^{obs}_{\rm max} = 6205$ d and $\Delta t^{obs}_{\rm max} = 0.25$ d). The PSD integral yields $\sigma^2_{\rm mod}$ for each mock AGN, which is then converted to $\sigma^2_{\rm obs}$ via equation (12). In the latter calculation we adopt $C = 1.3$ and $\beta = 1.1$, which are appropriate for the sampling pattern of the CDFS 7 Ms light curves. The selection function curve of Fig. 2 is used to assign weights to each mock AGN. The ensemble excess variance of the model AGN population within X-ray luminosity bins is the weighted average of the individual $\sigma^2_{\rm obs}$.

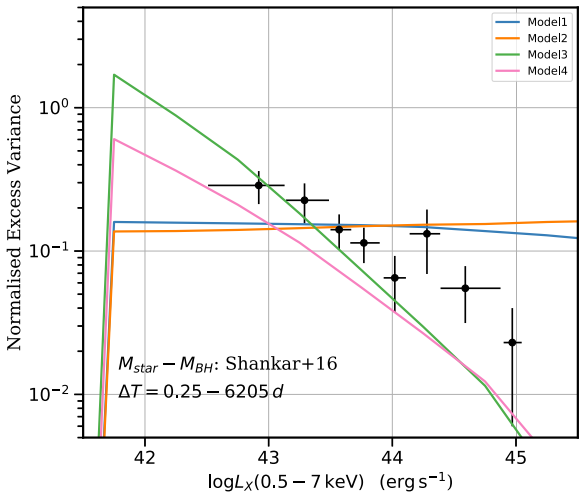

Figure 6. Normalized excess variance of AGN as a function of X-ray luminosity in the rest-frame 0.5–7 keV energy band. The data points are the measurements of the ensemble variance of the CDFS AGN in the redshift range $z = 0.4-4$ presented by Paolillo et al. (2017) for the longest time scale probed by these observations, 17 yr. The curves correspond to the empirical model presented in this paper for the four different parametrizations of the adopted PSD as indicated in the legend. These curves are based on the Shankar et al. (2016) 'unbiased' or 'intrinsic' stellar mass versus black hole mass scaling relation given by equations (2) and (3).

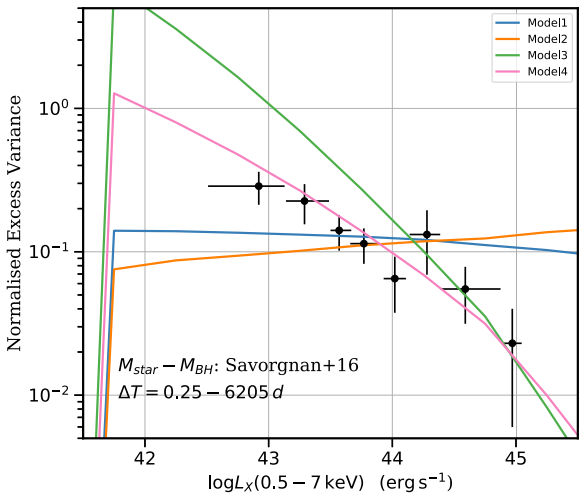

Figure 7. Same as Fig. 6 with the model curves constructed assuming the Savorgnan et al. (2016) dynamical stellar mass versus black hole mass scaling relation given by equation (1).

4 RESULTS

4.1 Model versus observations

The comparison of the CDFS ensemble variance observations with the model predictions is shown in Figs 6 and 7 for the Shankar et al. (2017) and Savorgnan et al. (2016) black hole mass versus stellar mass scaling relations respectively. The curves shown in these figures correspond to the four PSD models of Section 2.4. They predict very different relations between ensemble excess variance and luminosity. The PSD models 1 and 2 predict flat relations, whereas in models 3 and 4 the excess variance decreases with increasing luminosity. This is a result of the dependence of the PSD amplitude on Eddington ratio in the latter group of models. Fig. 8 shows that the mean Eddington ratio of mock AGN increases with increasing X-ray luminosity. This translates to a lower normalization of the corresponding PSDs (see equation 11) and hence, a lower ensemble excess variance with increasing luminosity. In contrast, the models 1, 2 are more rigid and the only variation in the excess variance of AGN is via the black hole mass dependence of the PSD break frequency. Fig. 9 shows the distribution of the black hole masses of mock AGN

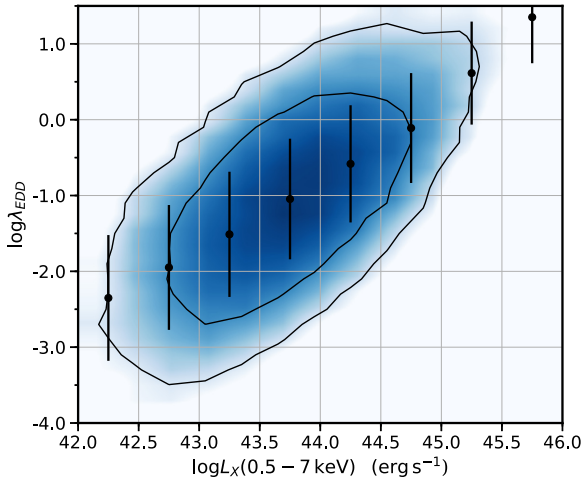

Figure 8. Eddington ratio as a function of the X-ray luminosity in the 0.5–7 keV band for the mock AGN sample that has been filtered through the 7 Ms-CDFS selection function of Fig. 2. The contours and the blue-shaded regions show the mock AGN distribution. Darker colours correspond to a higher density of sources. The contours enclose 68 and 95 per cent of the population. The data points and error bars show the mean and standard deviation of the Eddington ratio distribution in different luminosity bins. The Eddington ratio of mock AGN is estimated using the Savorgnan et al. (2016) black hole mass versus stellar mass scaling relation.

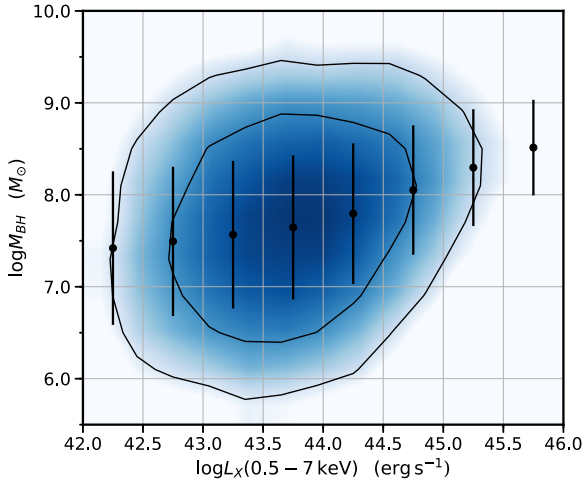

Figure 9. Black hole mass as a function of the X-ray luminosity in the 0.5–7 keV band for the mock AGN sample that has been filtered through the 7 Ms-CDFS selection function of Fig. 2. The contours and blue-shaded regions show the mock AGN distribution. Darker colours correspond to a higher density of sources. The contours enclose 68 and 95 per cent of the population. The data points and error bars show the mean and standard deviation of the black hole mass distribution in different luminosity bins. The black hole mass of mock AGN is estimated using the Savorgnan et al. (2016) black hole mass versus stellar mass scaling relation.

as a function of their X-ray luminosities. These two quantities are only weakly correlated in the sense that more luminous AGN are found in increasingly more massive black holes. This translates to a lower PSD break frequency with increasing luminosity. However, at fixed X-ray luminosity the median black hole mass only mildly increases with L_X. As a result for the variability time scales probed by the 7 Ms CDFS observations the black hole mass dependence of the PSD break frequency is insufficient to produce a strong drop in the ensemble excess variance of AGN towards bright luminosities.

The data points in Figs 6 and 7 show a decreasing trend with increasing luminosity and strongly favour the predictions of the PSD models 3 and 4. The flat excess variance curves produced by the models 1, 2 are inconsistent with these observations, irrespective of the black hole mass versus stellar mass relation. This result shows that the ensemble variance of AGN populations can constrain PSD models and points to a variable PSD amplitude that is a function of the physical parameters of the accretion process. This is in agreement with the results of Paolillo et al. (2017), who also favoured PSD models with amplitudes that depend on the accretion rate. However, the modelling presented by Paolillo et al. (2017) did not include any apriori constraints on the black hole masses of AGN, and therefore could not reject constant amplitude PSD models at a high confidence level. Our modelling approach links AGN demographics with variability models and therefore contains necessary additional information on the black hole mass distribution of AGN. The correlation between X-ray luminosity and black hole mass in our model (Fig. 9) is flatter than that assumed by Paolillo et al. (2017) and hence, provides stronger constraints on the PSD parametrization.

Figs 6 and 7 further show that the plotted model curves depend on the adopted stellar mass versus black hole mass scaling relation. At fixed redshift, X-ray luminosity, and PSD parametrization, there are differences between the models that use the Shankar et al. (2017) and the Savorgnan et al. (2016) $M_\star - M_{\rm BH}$ correlations. This indicates that measurements of the ensemble variability of AGN can constrain the $M_\star - M_{\rm BH}$ relation of the population. There is also evidence that the models 3, 4 provide a better representation of the observations in the case of the Savorgnan et al. (2016) scaling relation. The CDFS ensemble variability measurements therefore favour $M_\star - M_{\rm BH}$ relations based on dynamical black hole mass estimates.

The evidence above suggests that observations of the ensemble variance of AGN can jointly constrain PSD models and the relation between stellar and black hole mass of the population. Figs 6 and 7 provide important clues in this direction but do not explore the full range of model parameters that are consistent with the observations. Model inference is needed to sample the parameter space in a statistically robust way and provide confidence intervals to model parameters. This is also necessary to assign statistical significance to the results and allow the quantitative interpretation of the model parameters.

4.2 Model-parameter inference

We start by adopting simple parametric models for the $M_\star - M_{\rm BH}$ relation and the AGN PSD. Bayesian inference is then used to fit the observations of Fig. 6 and constrain the model parameters. The relation between stellar and black hole mass is parametrized as

$$\log M_{\rm BH} = \alpha + \beta \cdot (\log M_\star - 10). \quad (14)$$

The intrinsic scatter of this relation is fixed to 0.5 dex, i.e. comparable to that inferred by Shankar et al. (2017) and Savorgnan et al. (2016) for their scaling relations.

Table 1. Bayesian inference results for the parameters α β, γ, and δ of equations (14) and (15). The columns are (i) parameter name, (ii) the median value of the parameter and the corresponding uncertainty measured as the interval around the median that includes 68 per cent of the probability density, (iii) the type of prior, flat of Gaussian, used in the inference, and (iv) the prior range defined as the interval of the flat prior and the mean (μ), scatter (σ) of the Gaussian prior.

Parameter (1)	Median value and error (2)	Prior type (3)	Prior parameters (4)
α	$6.8^{+1.0}_{-1.1}$	Flat	[0–9]
β	$2.0^{+0.7}_{-1.0}$	Flat	[0–3]
γ	$-0.54^{+0.07}_{-0.09}$	Normal	$\mu = -0.8, \sigma = 0.15$
$\log \delta$	$-2.5^{+0.3}_{-0.3}$	Normal	$\mu = -2.522, \sigma = 0.2$

The adopted PSD parametrization is based on the Model 3 of Section 2.4. This is the simplest model that reproduces the observed luminosity dependence of the ensemble excess variance (see Figs 6 and 7). For the current inference application both the exponent and normalization are free parameters:

$$A = 2 \cdot \nu_{\rm b} \cdot PSD(\nu_{\rm b}) = \delta \cdot \lambda_{\rm Edd}^{\gamma}. \quad (15)$$

The AGN ensemble variability model therefore has a total of four free parameters, two related to the $M_\star - M_{\rm BH}$ relation (α, β) and the remaining (γ, δ) to the PSD model. We choose not to expand further the parameter space, e.g. by adding non-linear terms to equation (14) or allowing the scatter of this relation to be a free parameter. This is because the current observational constraints, although state of the art, still have relatively large uncertainties, which ultimately relate to small number statistics.

The free parameters α, β, γ, and δ are determined by sampling the likelihood

$$\mathcal{L} = -\frac{1}{2} \sum_i \frac{\left(\sigma^2_{{\rm NXV},i} - \sigma^2_{{\rm obs},i}\right)^2}{\delta^2_{{\rm NXV},i}}, \quad (16)$$

where $\sigma^2_{{\rm NXV},i}$ is the measured ensemble normalized excess variance for the X-ray luminosity bin i and $\delta^2_{{\rm NXV},i}$ is the corresponding uncertainty. The symbol $\sigma^2_{{\rm obs},i}$ is the ensemble excess variance predicted by the model for the luminosity bin i (equations 5 and 12). The likelihood above assumes that the excess variance measurements are normally distributed with a scatter that is represented by the corresponding uncertainty shown in Figs 6 and 7 (see Allevato et al. 2013). The MULTINEST multimodal nested sampling algorithm (Feroz & Hobson 2008; Feroz, Hobson & Bridges 2009) is used for parameter estimation. Flat priors are adopted for the model parameters α, β within the intervals 0–9 and 0–3, respectively. The choice of the priors for the parameters γ, δ is informed by results on the variability of local AGN presented by Ponti et al. (2012). They studied the excess variance of their sample as function of black hole mass and Eddington ratio and measured $\gamma = -0.8 \pm 0.15$ and $\delta = 0.003^{+0.002}_{-0.001}$. Based on these independent observational result we choose a Gaussian prior for γ with mean -0.8 and scatter $\sigma = 0.15$. The amplitude δ of the PSD can only take positive values. We therefore set a Gaussian prior for the parameter $\log \delta$ with a mean of $\log(0.003) = -2.522$ and scatter 0.20, which corresponds to the logarithmic uncertainty of the mean 1σ rms errors estimated by Ponti et al. (2012).

Table 1 lists the inference results for the four model parameters. Fig. 10 shows the corner plot of the parameter posterior distributions. There is a strong covariance between the slope, β and normalization,

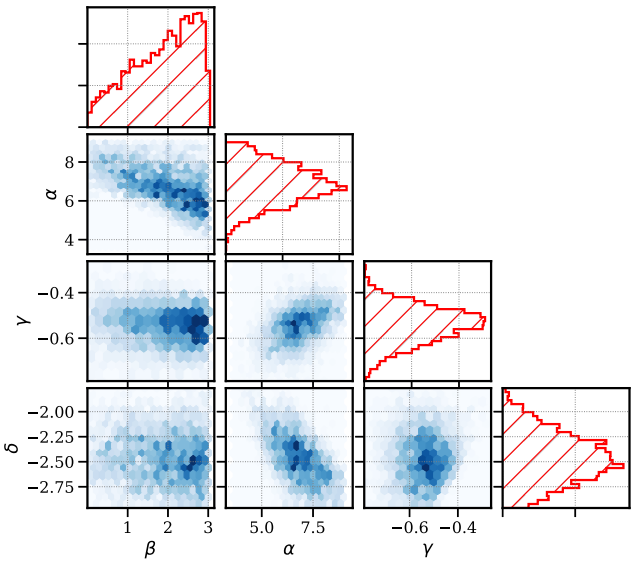

Figure 10. Corner plots of the posterior distributions of the parameters α, β, γ, and δ of the model presented in Section 4.2. These plots include both 2D and 1D projections of the posterior distribution.

α, of the scaling relation between black hole and stellar mass. Also, the slope β is largely unconstrained by the current ensemble variability observations. This is manifested by the broadness of the β posterior distribution, which is comparable to the adopted prior for this parameter (flat between 0 and 3). Aliases also exist between the parameters α and γ, in the sense that lower γ values broadly correspond to lower normalizations of the $M_\star - M_{\rm BH}$ relation. Based on the posterior distributions of Fig. 10 we find $\gamma = -0.54^{+0.07}_{-0.09}$ (Table 1), i.e. shallower than the prior $\gamma = -0.8 \pm 0.15$, which is estimated by Ponti et al. (2012) for local Seyferts. This shows that observations of the ensemble variance of AGN in deep survey fields provide additional information on the PSD of the population.

Also shown in Fig. 11 are the constraints on the $M_\star - M_{\rm BH}$ relation using the posterior distributions of the model parameters α, β of equation (14). The joint fit to the PSD and the $M_\star - M_{\rm BH}$ models produces results that are consistent with the scaling relation of Savorgnan et al. (2016). Nevertheless, the inferred 68 per cent confidence region around the median is broad and therefore the Shankar et al. (2017) relation cannot be excluded at a high confidence level. Improved ensemble variability measurements have the potential to provide better constraints on the $M_\star - M_{\rm BH}$ scaling relation of the AGN population and test different parametrizations proposed in the literature. For completeness, Fig. 11 also plots the projection of the model on to the observed space of the ensemble excess variance and X-ray luminosity.

The inferred parameters on the $M_\star - M_{\rm BH}$ relation in Table 1 are sensitive to the assumption that the stellar mass is a proxy to the bulge mass of galaxies. We explore the impact of this effect on the results by setting $M_{\rm bulge} = 0.5 \cdot M_\star$ for all mock AGN, i.e. similar to the bulge-to-total-mass ratio of Sb/Sbc-type galaxies (e.g. Fukugita et al. 1998; Oohama et al. 2009). The stellar mass, $M_\star$, in equation (14) is then substituted by the $M_{\rm bulge}$. This results to lower black hole masses and an overall lower $\sigma_{\rm obs}$ for the model AGN. Fitting the observations of Fig. 11 therefore requires a higher normalization of the $M_\star - M_{\rm BH}$ relation by about 0.5 dex. Observational constraints on the average $M_{\rm bulge}/M_\star$ ratio as a function of stellar massand redshift could help mitigate this systematic by including statistical corrections into the modelling.

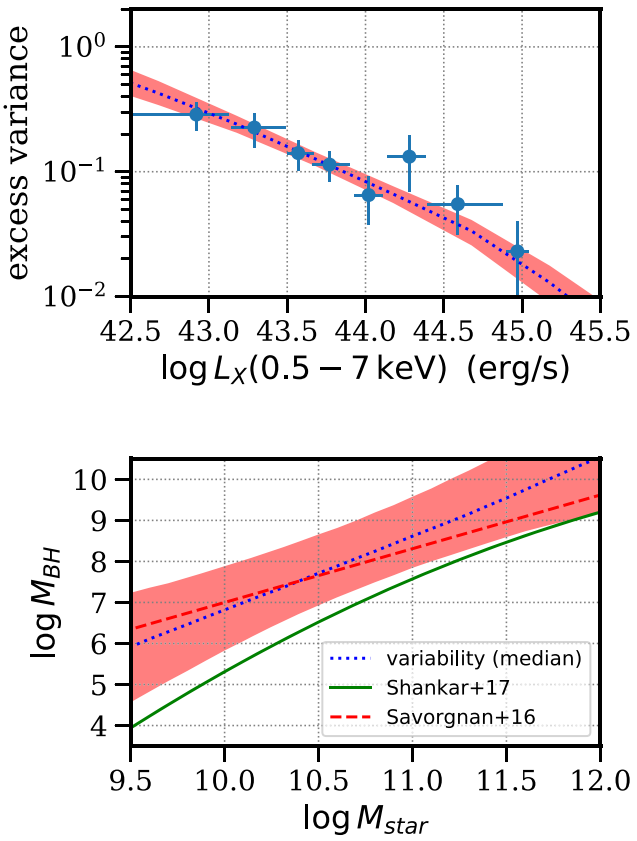

Figure 11. The top panel shows the projection of the model of Section 4.2 on to the $\sigma^2_{\rm NXV}$ versus L_X space. The data points are the measurements of the ensemble variance of the CDFS AGN in the redshift range $z = 0.4-4$ presented by Paolillo et al. (2017) for the longest time scale probed by these observations, 17 yr. The pink-shaded region is the model prediction using the posterior distributions shown in Fig. 10. The extent of the pink region corresponds to the 68 per cent confidence interval around the median. The bottom panel shows the $M_\star - M_{\rm BH}$ relation based on the posterior distribution of the parameters α, β (see equation 14). The blue dashed line shows the median at each $M_\star$ bin. The pink-shaded region corresponds to the 68 per cent confidence interval around the median. Also shown for comparison are the Savorgnan et al. (2016) dynamical stellar mass versus black hole mass relation (red-dashed line) and the Shankar et al. (2016) 'unbiased' or 'intrinsic' scaling relation (green solid curve).

4.3 Future prospects

Current measurements of the ensemble variance of AGN are limited by the size of the available samples. The number of extragalactic X-ray fields with sufficient number of multi-epoch observations is small. The eROSITA 4-year All Sky Survey (Predehl et al. 2020) will change this by providing 4-yr light curves with a 6-month cadence over a 4π solid angle. The large number of AGN in this survey combined with the modelling methodology described in this paper has the potential to provide unique joint constraints on the PSD and $M_\star - M_{\rm BH}$ relation as a function of redshift. The ensemble excess variance predicted by the model can generically be expressed as

$$\sigma^2_{\rm obs} = f(L_X, M_\star), \tag{17}$$

where we have assumed that the L_X is a proxy of the bolometric luminosity and the $M_\star$ is a measure of the black hole mass. The function $f(L_X, M_\star)$ encapsulates the dependence of the ensemble excess variance on the PSD model, the form of the $M_\star - M_{\rm BH}$ relation and the parametrization of the observational selection effects. The

equation above shows that the (L_X, $M_\star$) plane is the natural choice of parameter space for future ensemble variance measurements that are not limited by small number statitistics. Providing measurements of the $\sigma^2_{\rm NXV}$ in bins of stellar mass and accretion luminosity has the potential to minimize aliases between parameters of interest and improve the robustness of the results. Additionally, splitting samples into distinct redshift intervals can provide a handle on the cosmic evolution of, e.g. the $M_\star - M_{\rm BH}$ relation.

5 DISCUSSION AND CONCLUSIONS

A new model for the ensemble X-ray variability of AGN selected in extragalactic surveys is presented. It is developed upon empirical relations and is designed to account for observational selection effects, such as flux limits. The starting point of the model are observational measurements of the incidence of X-ray AGN among galaxies. These are combined with analytic expressions for the variability PSD of AGN and the $M_\star - M_{\rm BH}$ scaling relation to make predictions on the ensemble excess variance as a function of observables, such as accretion luminosity and redshift.

Comparison with observational measurements of the AGN ensemble excess variance (Paolillo et al. 2017) shows that the empirical model has predictive power and can constrain parameters related to, e.g. the AGN PSD and the $M_\star - M_{\rm BH}$ relation. Our modelling favours PSD models approximated by a double power law with amplitude that depends on the Eddington ratio and/or the black hole mass of the accreting system. Parametrizations of the PSD in which only the break frequency of the double power law depends on the physical properties of the AGN are unable to reproduce the observed decreasing trend of the ensemble excess variance with increasing X-ray luminosity. These constraints can feedback to studies of the light curves of individual local AGN (e.g. Ponti et al. 2012) to provide independent information on the PSD parametrization. Similar conclusions, but at lower significance, are presented by Paolillo et al. (2017).

An interesting feature of the empirical model developed in this paper is that it has the potential to constrain the black hole mass versus stellar mass relation of AGN samples based on measurements of their mean variability properties. This opens the possibility to constrain the redshift evolution of this relation and to complement studies that use spectral methods to directly measure black hole masses of QSO samples and relate them to the properties of their hosts (e.g. Treu, Malkan & Blandford 2004; Jahnke et al. 2009; Shen et al. 2015; Sexton et al. 2019; Li et al. 2021). We find that the ensemble variability observations of Paolillo et al. (2017) favour a normalization of the $M_\star - M_{\rm BH}$ relation similar to that measured in the local Universe for dormant black holes in quiescent spheroids (e.g. Kormendy & Ho 2013). Nevertheless the variability constraints shown in Fig. 11 cannot reject at a high confidence level a lower normalizations of the $M_\star - M_{\rm BH}$ relation proposed by Shankar et al. (2017). A substantial increase in the size of X-ray AGN samples with repeat observations is needed to improve current constraints and explore the redshift evolution of black hole/host-galaxy scaling relations. The eROSITA All Sky Survey has the potential to deliver such a data set.

DATA AND CODE AVAILABILITY

The code and data used in this paper are available at https://github.com/ageorgakakis/EnsembleVariability and https://zenodo.org/record/4725121.

ACKNOWLEDGEMENTS

We thank the referee for their careful reading of the paper and their constructive comments.

REFERENCES

Aird J., Coil A. L., Georgakakis A., Nandra K., Barro G., Pérez-González P. G., 2015, MNRAS, 451, 1892
Aird J., Coil A. L., Georgakakis A., 2018, MNRAS, 474, 1225
Aird J., Coil A. L., Georgakakis A., 2019, MNRAS, 484, 4360
Allevato V., Pinto C., Paolillo M., Papadakis I., Ranalli P., Comastri A., Iwasawa K., 2010, in Comastri A., Angelini L., Cappi M., eds, AIP Conf. Ser., Vol. 1248, X-ray Astronomy 2009; Present Status, Multi-Wavelength Approach and Future Perspectives. Am. Inst. Phys.,New York, p.491,
Allevato V., Paolillo M., Papadakis I., Pinto C., 2013, ApJ, 771, 9
Aversa R., Lapi A., de Zotti G., Shankar F., Danese L., 2015, ApJ, 810, 74
Azadi M. et al., 2015, ApJ, 806, 187
Bernardi M., Sheth R. K., Tundo E., Hyde J. B., 2007, ApJ, 660, 267
Brightman M., Nandra K., 2011, MNRAS, 414, 3084
Czerny B., Nikołajuk M., Piasecki M., Kuraszkiewicz J., 2001, MNRAS, 325, 865
Duras F. et al., 2020, A&A, 636, A73
Feroz F., Hobson M. P., 2008, MNRAS, 384, 449
Feroz F., Hobson M. P., Bridges M., 2009, MNRAS, 398, 1601
Fukugita M., Hogan C. J., Peebles P. J. E., 1998, ApJ, 503, 518
Georgakakis A., Aird J., Schulze A., Dwelly T., Salvato M., Nandra K., Merloni A., Schneider D. P., 2017, MNRAS, 471, 1976
Georgakakis A., Ruiz A., LaMassa S. M., 2020, MNRAS, 499, 710
Giacconi R. et al., 2002, ApJS, 139, 369
González-Martín O., Vaughan S., 2012, A&A, 544, A80
Gravity Collaboration, 2018, A&A, 618, L10
Gravity Collaboration, 2020, A&A, 635, A143
Ilbert O., et al., 2013, A&A, 556, A55
Jahnke K. et al., 2009, ApJ, 706, L215
Kauffmann G., Heckman T. M., 2009, MNRAS, 397, 135
Körding E. G., Migliari S., Fender R., Belloni T., Knigge C., McHardy I., 2007a, MNRAS, 380, 301
Körding E. G., Migliari S., Fender R., Belloni T., Knigge C., McHardy I., 2007b, MNRAS, 380, 301
Kormendy J., Ho L. C., 2013, ARA&A, 51, 511
Li J. I. H. et al., 2021, ApJ, 906, 103
Luo B. et al., 2017, ApJS, 228, 2
Lynden-Bell D., 1969, Nature, 223, 690
Markowitz A. et al., 2003, ApJ, 593, 96
McHardy I. M., Papadakis I. E., Uttley P., Page M. J., Mason K. O., 2004, MNRAS, 348, 783
McHardy I. M., Koerding E., Knigge C., Uttley P., Fender R. P., 2006, Nature, 444, 730
McHardy I. M., Arévalo P., Uttley P., Papadakis I. E., Summons D. P., Brinkmann W., Page M. J., 2007, MNRAS, 382, 985
Merloni A., Heinz S., 2008, MNRAS, 388, 1011
Nandra K., George I. M., Mushotzky R. F., Turner T. J., Yaqoob T., 1997, ApJ, 476, 70
Nikolajuk M., Papadakis I. E., Czerny B., 2004, MNRAS, 350, L26
Oohama N., Okamura S., Fukugita M., Yasuda N., Nakamura O., 2009, ApJ, 705, 245
Paolillo M., Schreier E. J., Giacconi R., Koekemoer A. M., Grogin N. A., 2004, ApJ, 611, 93
Paolillo M. et al., 2017, MNRAS, 471, 4398
Papadakis I. E., 2004, MNRAS, 348, 207
Papadakis I. E., Brinkmann W., Negoro H., Gliozzi M., 2002, A&A, 382, L1
Papadakis I. E., Chatzopoulos E., Athanasiadis D., Markowitz A., Georgantopoulos I., 2008, A&A, 487, 475
Ponti G., Papadakis I., Bianchi S., Guainazzi M., Matt G., Uttley P., Bonilla N. F., 2012, A&A, 542, A83
Predehl P. et al. 2021, 647, A1
Rees M. J., 1984, ARA&A, 22, 471

Sartori L. F., Schawinski K., Trakhtenbrot B., Caplar N., Treister E., Koss M. J., Urry C. M., Zhang C. E., 2018, MNRAS, 476, L34
Sartori L. F., Trakhtenbrot B., Schawinski K., Caplar N., Treister E., Zhang C., 2019, ApJ, 883, 139
Savorgnan G. A. D., Graham A. W., Marconi A. r., Sani E., 2016, ApJ, 817, 21
Scoville N., et al., 2007, ApJS, 172, 1
Sexton R. O., Canalizo G., Hiner K. D., Komossa S., Woo J.-H., Treister E., Hiner Dimassimo S. L., 2019, ApJ, 878, 101
Shankar F., Weinberg D. H., Miralda-Escudé J., 2013, MNRAS, 428, 421
Shankar F. et al., 2016, MNRAS, 460, 3119
Shankar F., Bernardi M., Sheth R. K., 2017, MNRAS, 466, 4029
Shankar F. et al., 2020, Nat. Astron., 4, 282
Shen Y. et al., 2015, ApJS, 216, 4
Treu T., Malkan M. A., Blandford R. D., 2004, ApJ, 615, L97
Uttley P., McHardy I. M., Papadakis I. E., 2002, MNRAS, 332, 231
Weigel A. K., Schawinski K., Bruderer C., 2016, MNRAS, 459, 2150

This paper has been typeset from a TEX/LATEX file prepared by the author.